Ab initio study of the oxidation on vicinal Si(001) surfaces: The step-selective oxidation

Jin-Nam Yeo, Gang Man Jee, and B. D. Yu*
Department of Physics, University of Seoul, Seoul 130-743, Korea

Hanchul Kim
Korea Research Institute of Standards and Science, P.O. Box 102, Yuseong, Daejeon 305-600, Korea

C.-H. Chung, H. W. Yeom, and I.-W. Lyo
Institute of Physics and Applied Physics, Yonsei University, 134 Shinchon, Seoul 120-749, Korea

Ki-jeong Kong
Korea Research Institute of Chemical Technology, P.O. Box 107, Yuseong, Daejeon 305-600, Korea

Y. Miyamoto
Nano Electronics Research Laboratories, NEC Corporation, 34 Miyukigaoka, Tsukuba 305-8501, Japan

O. Sugino
Institute for Solid State Physics, University of Tokyo, Kashiwa-shi, Chiba 277-8581, Japan

T. Ohno
National Institute for Materials Science, 1-2-1 Sengen, Tsukuba 305-0047, Japan
(Received 4 December 2006; revised manuscript received 10 August 2007; published 17 September 2007)

Initial oxygen adsorption structures and oxidation reaction on vicinal Si(001) surfaces with single-layer S_A and S_B steps were studied using *ab initio* total energy and electronic structure calculations. At the very early stage of the oxygen adsorption on Si(001), the calculations in this study show that oxygen atoms are preferentially incorporated into sites at the rebonded S_B step edge. Various stable oxidation structures at the rebonded S_B step were identified based on total energy calculations. Their stabilities are concerned with the structural attribute of the rebonded step-edge Si atoms (RSAs) with dangling bonds and weak rebonds. In addition, the proximity of the RSAs helps form the stable oxidation structures in high oxygen coverage regions that have in common a one-dimensional (1D) -Si-O- chain structure along the step edge as a basic 1D oxide building element. By forming this 1D chain structure, it is possible to effectively reduce the number of dangling bonds (DBs) at the step edge. This indicates that the reduction of the number of step-edge DBs plays a crucial role in the formation of oxidation complexes at the steps with local strain, as seen on flat semiconducting surfaces. For more detailed information, the electronic properties of the oxidation complexes were also calculated. The calculated site-projected density of states and scanning tunneling microscopy images of the oxidation structures exhibit characteristic features distinct from those of the clean vicinal Si surface. All these results clearly show that the S_B step acts as a strong sink for the oxidation of Si as suggested in experiments.

DOI: 10.1103/PhysRevB.76.115317 PACS number(s): 68.43.−h, 81.16.−c, 81.10.Aj

I. INTRODUCTION

The formation of ultrathin oxide films on silicon surfaces has attracted much attention as one of the most important processes in the technological development of future Si-based electronic devices with sizes reduced.[1] Particularly, the precise control of the surface oxidation for better functioning Si devices requires deep understanding of the initial reaction of oxygen to Si surfaces on an atomic scale.

There have been extensive studies on the early stage of oxidation such as oxidation structures, elementary oxidation processes, and initial growth modes, using various experimental techniques and theoretical methods.[2–32] Many experimental and theoretical works show that surface Si dimer atoms play a crucial role in initial oxidation processes on flat terraces of Si(001). However, when surfaces become complicated by nanostructures such as step edges, an understanding of the initial oxidation processes has remained elusive.

On Si(001) surfaces, it is well known that surface Si atoms reconstruct by forming dimers and the dimers are aligned in parallel rows. As a result of the dimerization, the orientation of the reconstruction alternates on terraces separated by single-layer steps.[33] There are two distinct types of single-layer steps on vicinal Si(001) surfaces: one with the dimer rows on the upper terrace oriented parallel to the step edge and the other with the dimer rows on the upper terrace oriented perpendicular to the step edge, which are denoted by S_A and S_B, respectively, following Chadi[33] (see Fig. 1). For the S_A step, the local configurations of the step-edge atoms resemble those of the Si dimer atoms on flat terraces. In contrast, for the S_B step, there is a possibility of forming rebonded structures of Si pentagons at the step edge by having step-edge Si atoms rebond to the second-layer Si atoms on the upper terrace [see Fig. 1(b)], which effectively helps in reducing the number of dangling bonds (DBs) at the step edge. The rebonded S_B step exhibits electronic structures dis-

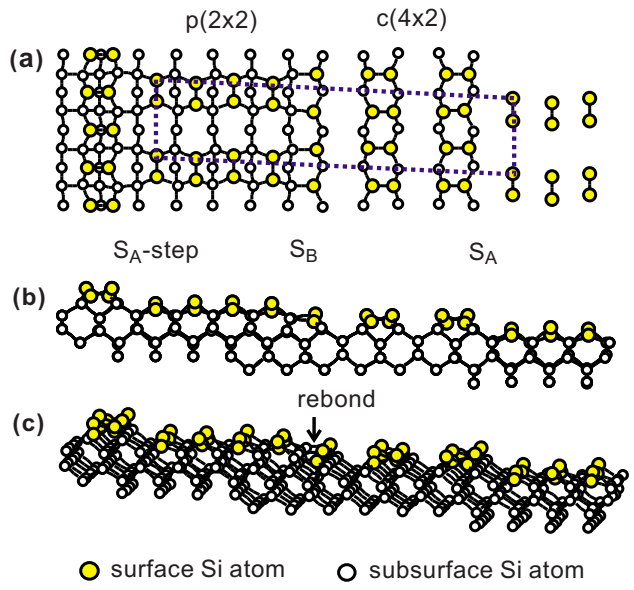

FIG. 1. (Color online) Atomic structure of a (1,1,19) Si surface that is vicinal to (001): (a) top, (b) side, and (c) perspective views. There are two types of single-layer steps that exhibit the alternate orientation of the dimer reconstruction on terraces.

tinct from those exhibited by the Si dimer atoms on flat terraces, as shown by scanning tunneling microscopy (STM) and scanning tunneling spectroscopy (STS).[34,35] Previous works showed that this S_B step acts as a strong sink for Si adatoms in the homoepitaxial growth of Si.[36] At the very early stage of oxygen adsorption on Si(001), the rebonded S_B step is also expected to play an active role.

STM measurements have been instrumental in the understanding of initial oxidation reaction processes on Si(001) surfaces. Avouris and Cahill reported experimental observations that oxygen molecules preferentially react to the rebonded S_B step edge during the adsorption of oxygen on Si(001).[15] More recently, Chung *et al.*[32] studied the initial oxidation processes on ultraclean Si(001)-$c(4\times2)$ surfaces by using STM at a temperature as low as 80 K. In the experiment, ultraclean Si surfaces with no *C*-type defects and very low density of *A*- and *B*-type defects were used to minimize the effect of the defects. Through such experimental efforts, the atomically resolved STM information on the very strong selective oxidation at the rebonded S_B step was obtained.

In this paper, possible oxygen adsorption structures and oxidation reaction on vicinal Si(001) surfaces with single-layer steps were studied using *ab initio* total energy and electronic structure calculations based on density-functional theory (DFT),[37] which extends the work previously presented.[32] The calculations show that oxygen atoms are preferentially incorporated into sites at the S_B step edge consisting of rebonded Si atoms. The binding energies are much higher than those on the flat terraces and at the S_A step. The very strong reactivity of the step edge is attributed to the presence of rebonded step-edge Si atoms with DBs and weak rebonds. The proximity of the rebonded step-edge Si atoms also allows the formation of a -Si-O- chain structure along the step edge in high oxygen coverage regions, thereby effectively eliminating the energetically unprofitable step-edge DBs. The local electronic structures and STM images for the oxidation structures presented in this work were also determined. All these results provide a natural explanation of the experimental observation that the rebonded step edge acts as a strong sink for the oxidation of Si.

This paper is organized as follows. In Sec. II, the method of calculations is described. The results and discussion are presented in Sec. III. Finally, the paper is summarized in Sec. IV.

II. CALCULATION METHOD

All calculations were performed using the DFT[37] and the Vanderbilt ultrasoft pseudopotentials[38,39] as implemented in the Vienna *ab initio* simulation package.[40,41] DFT calculations were performed within the generalized gradient approximation (GGA) of the exchange and correlation functional.[42] Wave functions were expanded in terms of the plane-wave basis set with a cutoff energy of 260 eV.

To simulate the adsorption of oxygen on vicinal Si(001) surfaces, a (1,1,19) vicinal surface was used that contains alternate single-layer S_A and S_B steps in a calculational unit cell (see Fig. 1).[43,44] The surface unit cell used in the calculations is represented by the dashed lines in Fig. 1(a). The surface was modeled by the repeating slab structure consisting of six Si layers with the 8.0 Å vacuum region. For the Si slab, the theoretical GGA lattice constant a_0=5.46 Å of bulk Si was used. The **k**-space integration was done with a summation over the uniform mesh of 4 **k** points in the surface Brillouin zone of the supercell. The bottom Si atoms of the slab were terminated by hydrogen atoms. The atoms in the top five Si layers and the oxygen adatoms were relaxed.[30] All the geometries in this study were optimized until the remaining forces were smaller than 0.02 eV/Å.

III. RESULTS AND DISCUSSION

A. Atomic structures and energetics

For the (1,1,19) vicinal surface used in our calculations, periodicity along the step edge was set to be double surface lattice constants: As such, the geometry-optimized surface structure consists of (001) terraces, which have alternate $p(2\times2)$ and $c(4\times2)$ reconstructed structures [see Fig. 1(a)]. On each terrace, the orientation of the reconstruction is different, resulting in the formation of alternate single-layer S_A and S_B steps.[33] At the S_A step, local atomic configurations of step-edge dimers are very similar to those of Si dimers on flat terraces. As a result, the formation of the S_A step does not produce significant strain or extra dangling bonds at step edges. In contrast, at the S_B step, the step-edge Si atoms rebond to the second-layer Si atoms on the upper terrace to reduce the number of the Si DBs at the step edge [see Fig. 1(c)]. The rebonded step-edge Si atoms (RSAs) buckle alternately up and down along the step-edge direction by transferring electrons from the down RSA to the up RSA to further reduce the energy. The sum of the bond angles of the down RSA is 349° close to 360° of the sp^2 configuration. As

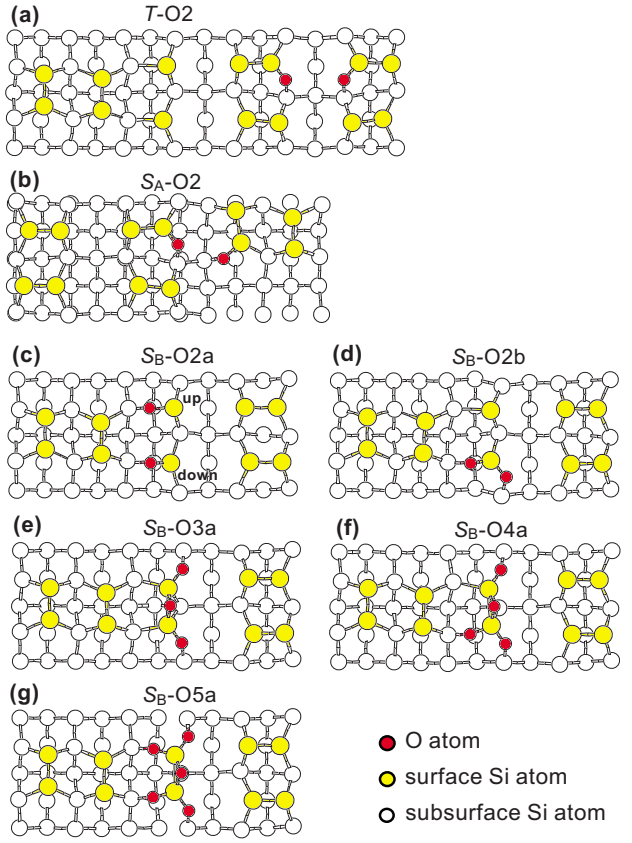

FIG. 2. (Color online) Various oxidation structures at flat terraces, S_A, and rebonded S_B steps. In each structural view, the right half corresponds to the lower terrace.

such, the down RSA becomes positively charged. The rebonds at the S_B step edge are weaker compared with the dimer bonds on flat terraces; the calculated rebond distances of the up and down step-edge Si atoms are 2.54 and 2.44 Å, respectively, larger than those of the Si dimer atoms on the flat terrace (2.35 Å).

For the flat (001) terrace, the $c(4\times2)$ surface structure that has the lowest energy in our total energy calculations was used. On the $c(4\times2)$ terrace, the primary oxidation structure with two oxygen adatoms in the unit cell is the model structure with one atom at the backbond site of the down dimer atom and the other at the backbond site of the down dimer atom on the neighboring dimer row. This is the model proposed by Kato *et al.*[26] [see Fig. 2(a)]. The oxidation structures are denoted by *X*-O*n*y herein. The letter *X* specifies adsorption places such as terraces (*T*), and S_A and S_B steps. The number *n* denotes the number of oxygen adatoms in the unit cell. The letter *y* was used to specify the different configurations with the same *X* and *n*. The model of Kato *et al.* is herein called backbond site *T*-O2. Near the S_A step, the two oxygen atoms can also react to the down Si dimer atoms on the upper and lower terraces, respectively, and each oxygen atom was incorporated into the backbond site. This structure is called S_A-O2 [see Fig. 2(b)].

The calculated Si-O bond lengths $\ell_{\text{Si-O}}$, Si-Si distances $\ell_{\text{Si-(O)-Si}}$, and bond angles of oxygen adatoms $\theta_{\text{Si-O-Si}}$ for the Si-O-Si bonds at those sites are summarized in Table I.

TABLE I. Calculated structural parameters for the various stable oxygen adsorption structures. Here, $\ell_{\text{Si-O}}$ is the Si-O bond length, $\ell_{\text{Si-(O)-Si}}$ the Si-Si distance in the Si-O-Si bonds, and $\theta_{\text{Si-O-Si}}$ the bond angle of the oxygen atom. Numbers in each structural model were arranged to match the Si-O-Si bonds in the top-to-bottom order for the corresponding Si-O-Si positions in Fig. 2.

Oxidation structures	$\ell_{\text{Si-O}}$ (Å)	$\ell_{\text{Si-(O)-Si}}$ (Å)	$\theta_{\text{Si-O-Si}}$ (deg)
T-O2	1.63, 1.71	2.84	116
	1.64, 1.71	2.82	114
S_A-O2	1.63, 1.71	2.84	116
	1.64, 1.70	3.00	128
S_B-O2a	1.72, 1.65	3.24	148
	1.65, 1.74	3.10	132
S_B-O2b	1.61, 1.75	3.05	130
	1.61, 1.76	2.74	109
S_B-O3a	1.69, 1.65	2.94	124
	1.70, 1.72	2.61	100
	1.65, 1.68	2.94	123
S_B-O4a	1.68, 1.64	2.99	129
	1.71, 1.70	2.60	99
	1.65, 1.69	3.09	136
	1.64, 1.69	2.91	122
S_B-O5a	1.68, 1.63	2.95	126
	1.68, 1.66	3.11	138
	1.69, 1.70	2.56	98
	1.65, 1.69	3.14	140
	1.63, 1.68	2.94	125

Figure 3 shows the calculated adsorption energy per oxygen adatom E_{ad}(*X*-O*n*y) for the configuration *X*-O*n*y, which is defined as follows: $E_{\text{ad}}(X\text{-O}n\text{y})=[E(X\text{-O}n\text{y})-E(\text{clean surface})-nE_{\text{O}}]/n$. Here, $E(X\text{-O}n\text{y})$ is the total energy of the configuration *X*-O*n*y, *n* the number of oxygen adatoms in the unit cell, and E_{O} the spin-polarized total energy of a free oxygen atom. Our total energy calculations showed that the S_A-O2 structure at the S_A step is by 0.10 eV/adatom more stable than the *T*-O2 structure.

In addition to the above oxidation models on the terrace and at the S_A step, other possible oxidation structures with two oxygen adatoms in the unit cell were also considered at the S_B step with the RSAs. Two representative stable oxidation structures were found: S_B-O2a [Fig. 2(c)] and S_B-O2b [Fig. 2(d)]. In the S_B-O2a structure, the dissociated oxygen atoms were incorporated into the rebond-bridge sites of the S_B step. In the S_B-O2b structure, oxygen atoms react to the down RSA: One oxygen atom is located at the rebond-bridge site of the down RSA as in the S_B-O2a structure and the other oxygen atom at the backbond site of the same down RSA [Fig. 2(d)]. Interestingly, the two oxidation structures at the rebonded S_B step were found to be more stable than the oxidation structures on the terrace and at the S_A step. The

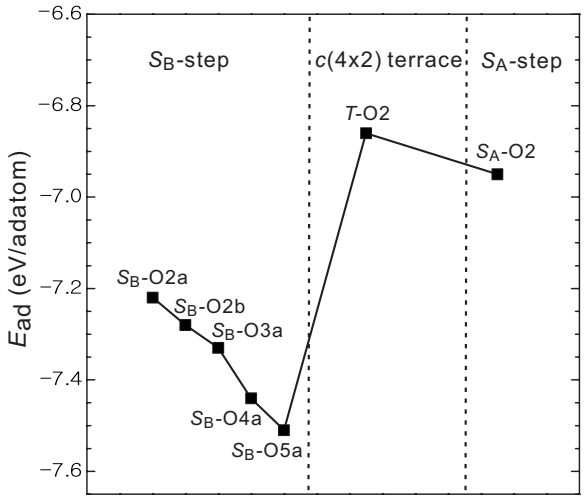

FIG. 3. Calculated adsorption energies E_{ad} per oxygen adatom for the various stable oxidation structures on the vicinal Si(001) surface.

adsorption energies of S_B-O2a and S_B-O2b structures are lower by 0.36 and 0.42 eV/adatom, respectively, than that of the *T*-O2 structure (Fig. 3). The S_B-O2b structure is slightly more favored by 0.06 eV/adatom than the S_B-O2a structure. This indicates that the S_B-O2a and S_B-O2b oxidation structures at the S_B step are preferentially formed in lower oxygen coverage regions.

In addition to oxidation structures of S_B-O2a and S_B-O2b at the rebonded S_B step, oxidation structures shown in Fig. 4 were also considered herein and adsorption energies are summarized in Table II. Among them, the oxidation structure S_B-O2c was also found to be stable and the energy was only 0.03 eV/adatom higher than that of the most stable S_B-O2b

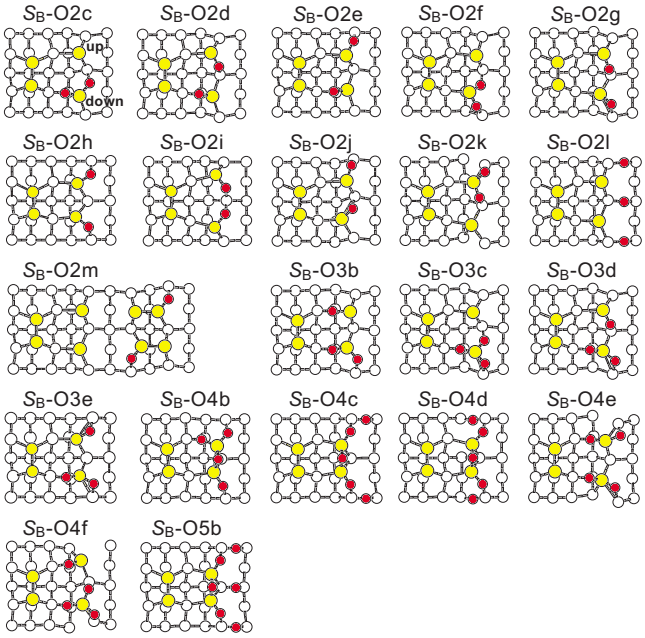

FIG. 4. (Color online) Other oxidation structures at the rebonded S_B step.

TABLE II. Calculated adsorption energies E_{ad} for the various oxidation structures at the S_B step edge. The relative adsorption energies ΔE_{ad} to that of the most stable oxidation structure are also given for each number of oxygen adatoms in the unit cell.

Oxidation structures	E_{ad} (eV/adatom)	ΔE_{ad} (eV/adatom)
T-O2	−6.86	0.42
S_B-O2a	−7.22	0.06
S_B-O2b	−7.28	0.00
S_B-O2c	−7.25	0.03
S_B-O2d	−6.96	0.32
S_B-O2e	−6.96	0.32
S_B-O2f	−6.71	0.57
S_B-O2g	−6.53	0.75
S_B-O2h	−6.59	0.69
S_B-O2i	−6.66	0.62
S_B-O2j	−6.53	0.75
S_B-O2k	−6.42	0.86
S_B-O2l	−7.11	0.17
S_B-O2m	−6.89	0.39
S_B-O3a	−7.33	0.00
S_B-O3b	−7.15	0.18
S_B-O3c	−6.90	0.43
S_B-O3d	−6.91	0.42
S_B-O3e	−6.83	0.50
S_B-O4a	−7.44	0.00
S_B-O4b	−7.39	0.05
S_B-O4c	−7.41	0.03
S_B-O4d	−7.34	0.10
S_B-O4e	−7.05	0.39
S_B-O4f	−7.01	0.43
S_B-O5a	−7.51	0.00
S_B-O5b	−7.31	0.20

structure. The structural and electronic properties of S_B-O2c were very similar to those of S_B-O2b, so the S_B-O2c structure was not further described separately herein. The other structures except for S_B-O2c were found to be much higher in energy than the S_B-O2a, S_B-O2b, and S_B-O2c structures (see Table II). A close inspection of oxidation structures showed that the adsorption of the oxygen adatom in the weak rebond bridge of the positively charged down RSA is the common, important factor for stabilizing the S_B-O2a, S_B-O2b, and S_B-O2c structures in lower oxygen coverage regions. At this adsorption site, it costs lesser energy to break the weak rebond and form the Si-O-Si bonds than with the normal Si-Si bond. The oxygen adatom favors sitting at sites near the positively charged down RSA like the oxygen adatom on the dimerized, flat Si(001) surface. This finding provides a natural explanation for the favorable formation of the stable S_B-O2a, S_B-O2b, and S_B-O2c structures at the rebonded S_B step. Such a role of the rebonds in the adsorption of

oxygen was not considered in previous studies[45,46] of the oxidation on nonrebonded vicinal Si(001) surfaces.

In regions of higher oxygen coverage, possible oxidation structures at the rebonded S_B step were also considered. The total energy calculations that were made showed that the oxidation structures of S_B-O3a, S_B-O4a, and S_B-O5a are the energetically most stable ones among structures with three, four, and five oxygen atoms per unit cell, respectively. The geometry-optimized structures of S_B-O3a, S_B-O4a, and S_B-O5a are shown in Fig. 2. In the S_B-O3a structure, which is the model proposed by Yu *et al.*,[31] two oxygen atoms are located at the backbond sites of the two RSAs and the oxygen atom at the inter-RSA bridge site. As such, they form a -Si-O-chain structure that effectively eliminates the energetically unprofitable step-edge DBs. The S_B-O4a structure is a combination of the S_B-O3a unit and the other oxygen atom at the rebond-bridge site of the down RSA at the S_B step [Fig. 2(f)]. The S_B-O5a structure is obtained by combining the S_B-O3a unit and the two additional oxygen atoms at the rebond-bridge sites of the two RSAs at the S_B step.

The adsorption energy calculations in Fig. 3 showed that the silicon oxide formation becomes more favorable with more oxygen adatoms. The adsorption energies of oxidation structures S_B-O3a, S_B-O4a, and S_B-O5a are lower by 0.47, 0.58, and 0.65 eV/adatom than that of the T-O2 structure, respectively. Interestingly, all high oxidation structures have the S_B-O3a structural unit in common in which the oxygen atom bridges the two RSAs to eliminate the energetically unfavorable step-edge DBs. Further inspection of the optimized atomic geometries of S_B-O3a, S_B-O4a, and S_B-O5a shows that such a chain structure, however, significantly weakens the buckling of the RSAs that is energetically profitable on the clean vicinal surface. It is also noted that the Si-O-Si bond angles of the oxygen atom at the inter-RSA bridge site are near 100°, smaller than those for the other Si-O-Si bonds (see Table I). It is concluded that the reduction in the number of DBs plays a crucial role in determining the oxidation structures even at the rebonded S_B step edge with local strain, as seen on many semiconducting surfaces.

In addition to the high oxidation structures of S_B-O3a, S_B-O4a, S_B-O5a at the rebonded S_B step, oxidation structures shown in Fig. 4 were also considered herein and Table II summarizes the adsorption energies. For the oxidation structure with four oxygen adatoms in the unit cell, the S_B-O4b and S_B-O4c structures were also found to be stable and the energies were only 0.05 and 0.03 eV/adatom higher than that of the most stable S_B-O4a structure, respectively. The structural and electronic properties of the S_B-O4b and S_B-O4c structures were similar to those of S_B-O4a, so they are not further mentioned herein like S_B-O2c. All the other high oxidation structures in Fig. 4 except for S_B-O4b and S_B-O4c were found to be much higher in energy than the S_B-O3a, S_B-O4a, and S_B-O5a structures.

B. Electronic structures

The electronic structures of the various oxidation structures determined in this work were analyzed through the Si-site-projected densities of states (PDOSs). The PDOS features obtained in this way can be used in gaining an understanding of the origin of corrugation in experimental STM images and furthermore to predict and complement experimental observations as the PDOS analysis delineates individual atom contributions.

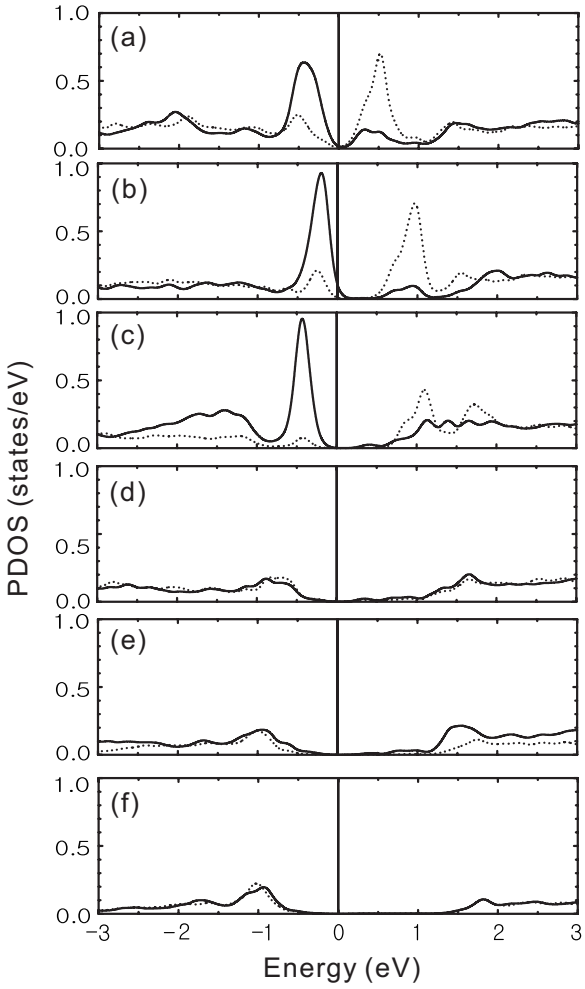

FIG. 5. Site-projected densities of states (PDOS) of the RSAs for (a) the clean vicinal surface, (b) S_B-O2a, (c) S_B-O2b, (d) S_B-O3a, (e) S_B-O4a, and (f) S_B-O5a structures. The solid and dotted lines represent the PDOS of the up and down RSAs, respectively. The energy zero is set at the Fermi energy E_F.

Figures 5(a)–5(f) present the PDOS of the up and down RSAs for the clean vicinal surface, S_B-O2a, S_B-O2b, S_B-O3a, S_B-O4a, and S_B-O5a structures, respectively. For the clean vicinal surface, the PDOS showed peaks at −0.4 and +0.5 eV. The peaks in the filled and empty states are assigned to the localized electronic states of the up and down RSAs herein, respectively [Fig. 5(a)]. Such a peak in the local density of states for the empty state at +0.5 eV was observed in previous STM and STS studies.[32,34,35] For the S_B-O2a structure, the empty-state peak at +0.5 eV in the PDOS of the clean vicinal surface is by 0.4 eV shifted upward on the energy scale [Fig. 5(b)]. The PDOS of the S_B-O2b structure shows that the empty-state peak near the Fermi energy is significantly weakened compared with that of the clean vicinal surface [Fig. 5(c)].

When additional oxygen adatoms are introduced, the most stable oxidation structures are the S_B-O3a, S_B-O4a, and S_B-O5a structures that have in common the -Si-O- chain along the rebonded S_B step edge. The PDOS of the S_B-O3a, S_B-O4a, and S_B-O5a structures are obviously affected by the formation of the -Si-O- chain that eliminates the step-edge DBs of the up and down RSAs. Indeed, the peak features in the region near the Fermi energy corresponding to the DBs of the RSAs are significantly reduced [Figs. 5(d)–5(f)].

As mentioned above, the step-selective incorporation of oxygen into the RSAs proceeds to high oxidation structures by forming the unique, unusual one-dimensional (1D) silicon oxide chain along the step edge. As such, the high oxidation structures are expected to have the physical properties of the 1D silicon oxide in common. For the high oxidation structures, the PDOSs were found to be very small in the vicinity of the Fermi energy [Figs. 5(d)–5(f)]. Notably the energy gaps at the RSAs widen with the increase of the oxidation level, indicating that they are indeed subnanometer-scale insulators.

C. Calculated scanning tunneling microscopy images

STM images for the oxygen-reacted structures at the rebonded S_B step have been calculated at various bias voltages. They can be compared to the experimental STM images that show atomic resolution on these surfaces. The clean vicinal surface was previously studied by Komura *et al.*[34,35] They observed bright protrusions at the rebonded S_B step prominent at empty-state images. Chung *et al.*[32] reported that the observation is limited to the bias window from zero to about +1.5 V. Such features were reproduced well in the corresponding theoretical STM simulations. At the empty-state images of sample bias voltages $V_S = +0.5, +0.7$ V, the two bright protrusions were obtained [Figs. 6(a) and 6(b)]: A circular bright protrusion (A) at the step-edge dimer on the upper terrace, and a fuzzy bright protrusion (B) at the RSAs. In the images of the empty state with bias voltages higher than 1.0 V, and of the filled state, however, these features were not obtained [Figs. 6(c) and 6(d)]. This agrees well with the PDOS of the clean vicinal surface in Fig. 5(a). It should be here noted that the DFT calculations underestimate the gap values in semiconductors. That explains why the theoretical images of the bright protrusions were obtained at +0.5 and +0.7 V lower than +1.2 and +1.0 V in the experiments.[32,34,35]

For oxidized Si(001) surfaces, Chung *et al.*[32] reported that both types of the bright protrusions observable in the empty state of the pristine S_B step were affected in proportion to the oxygen dose. Figure 7 shows the simulated STM images for the S_B-O2a and S_B-O2b structures after the reaction of the RSAs to the oxygen atoms. With the oxygen atoms included in the S_B step, the bright protrusion [A in Fig. 6(a)] at the step-edge dimer on the upper terrace split into two less bright spots [C and D in Figs. 7(a) and 7(c), respectively] with a dark node in the middle of the step-edge dimer. At the RSA sites, the fuzzy bright protrusion [B in Fig. 6(a)] disappeared, and instead alternate bright and dark images were obtained.

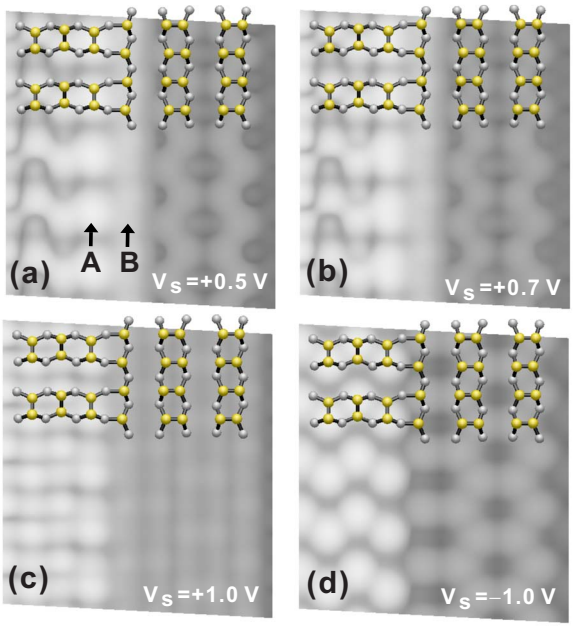

FIG. 6. (Color online) Simulated STM images at the rebonded S_B step for the clean vicinal Si(001) surface at various sample bias voltages V_S: [(a)–(c)] empty-state and (d) filled-state images. In each image, the right half corresponds to the lower terrace.

It was also found that at sample bias voltages higher than 1.0 V, the simulated filled- and empty-state STM images for the S_B-O2a and S_B-O2b structures were indistinguishable from those of the clean vicinal surface [Figs. 7(b) and 7(d)]. All these features agree well with the experimental observations in the oxygen dose of 0.12 L by Chung *et al.*[32]

The STM studies of Chung *et al.*[32] also reported that at a higher oxygen dose dark trench images were observed along

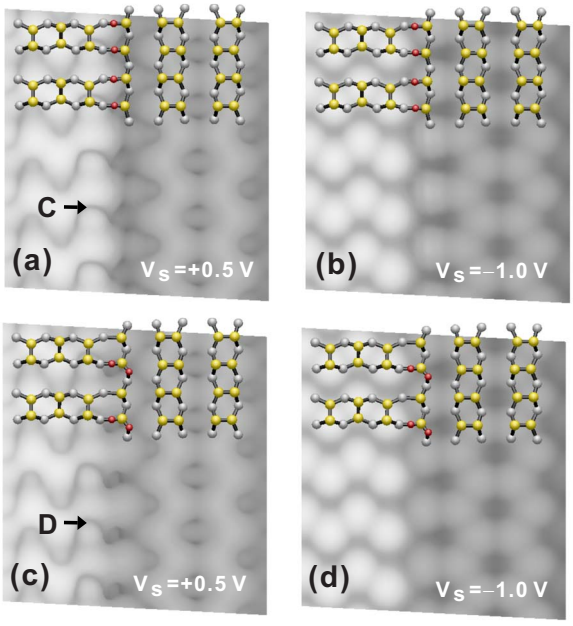

FIG. 7. (Color online) Simulated empty- and filled-state STM images: [(a) and (b)] S_B-O2a and [(c) and (d)] S_B-O2a structures.

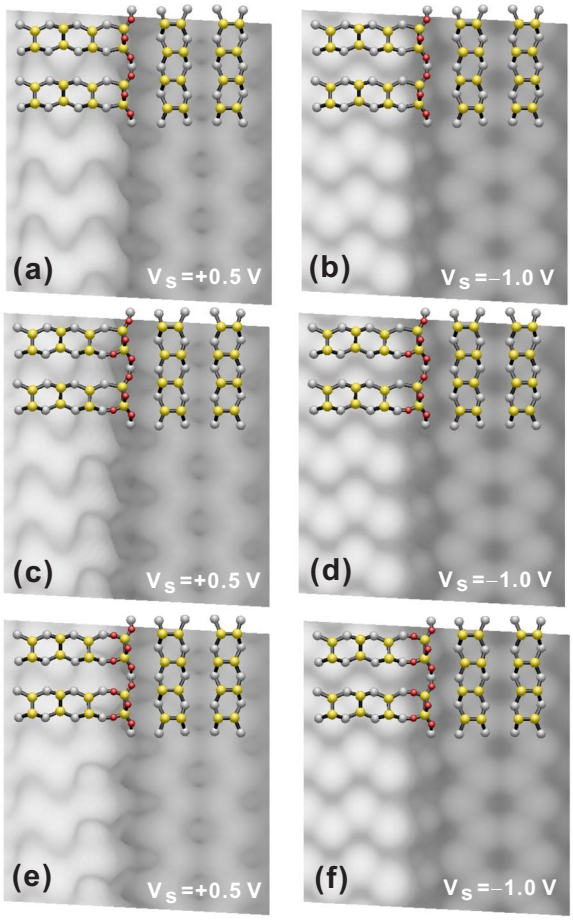

FIG. 8. (Color online) Simulated empty- and filled-state STM images: [(a) and (b)] S_B-O3a, [(c) and (d)] S_B-O4a, and [(e) and (f)] S_B-O5a structures.

the S_B step edge in both empty- and filled-state STM images. These images were different from those of the oxidation structures S_B-O2a and S_B-O2b at the rebond sites of the RSAs. Figure 8 shows the simulated STM images of the S_B-O3a, S_B-O4a, and S_B-O5a structures theoretically determined in the higher oxygen coverage regions. The images of a dark trench line along the step edge were found in both empty- and filled-state simulated images of S_B-O3a, S_B-O4a, and S_B-O5a in agreement with experimental observations. These features can be also expected to appear from the significantly weakened PDOS near the Fermi energy of the higher oxidation structures, S_B-O3a, S_B-O4a, and S_B-O5a [Figs. 5(d)–5(f)], where the oxygen atom bridges the two RSAs to reduce the local density of states of the DBs at the rebonded S_B step edge. The appearance of the dark trench is clearly discernible from the STM images of the clean vicinal surface and of the S_B-O2a and S_B-O2b structures. Considering the good agreement between the first-principles and experimental STM images, the dark trench essentially represents the higher oxidation states with no DBs and the emergence of an insulating phase at the S_B step.

IV. SUMMARY

The incorporation structures and atomic processes of oxygen atoms on vicinal Si(001) surfaces during the initial stages of silicon oxide growth were investigated by carrying out *ab initio* total energy and electronic structure calculations based on the density-functional theory. The calculations showed that oxygen atoms are preferentially incorporated into the sites of the rebonded step-edge Si atoms (RSAs) at the S_B step. This finding agrees well with the findings of previous STM studies.[15,32] The resulting oxidation structures S_B-O2a and S_B-O2b in lower oxygen coverage regions were by 0.36 and 0.42 eV/adatom more stable than the backbond oxidation structure on the flat terrace T-O2, respectively. It is herein noted that the rebond Si atoms at the S_B step edge are in part structurally very similar to the Si adatoms on a Si(111)-7×7 surface that have one DB and three backbonds with underlying subsurface Si atoms. The structural similarity of the S_B-O2b structure and the oxidation product of the adatoms on Si(111)-7×7 looks quite reasonable.[47]

Further inspection of the atomic geometry of the clean vicinal Si(001) surface showed that the rebonds at the S_B step are significantly elongated compared to the atomic bonds in bulk Si as much as 0.2 Å. As such, the RSAs become more flexible with respect to oxygen-induced strains. Indeed, in higher oxidation coverage regions, the adsorbed oxygen atom successfully bridges the neighboring RSAs to effectively eliminate the DBs at the rebonded step edge, finally forming the -Si-O- chain structure along the step edge that is energetically very profitable. This unique, unusual one-dimensional (1D) alignment of silicon oxides was never observed on other surfaces, even for the Si(111)-7×7 surface mentioned above. This 1D silicon oxide structure, called S_B-O3a herein, constitutes a basic building unit for the higher oxidation structures S_B-O4a and S_B-O5a. The S_B-O3a, S_B-O4a, and S_B-O5a structures were by 0.47, 0.58, and 0.65 eV/adatom more stable than the T-O2 structure, respectively.

For the stable oxidation structures determined in this work, electronic properties were also investigated by calculating site-projected densities of states (PDOSs) and STM images. The adsorption of oxygen atoms significantly affects the electronic structures of the atoms near the S_B step with the RSAs. The calculations of the PDOS and STM images exhibit features that are distinct from those of the clean S_B step. The good agreement between the simulated and experimental STM images indicates that the dark trenches experimentally observed near the S_B step essentially represent the higher oxidation structures S_B-O3a, S_B-O4a, and S_B-O5a with the DBs of the RSAs passivated.

In conclusion, the calculation results and analysis of the preferential oxidation at the S_B step presented in this work reveal not only a crucial role of the rebonded step edge in the oxidation reaction of Si(001) surfaces but also the formation of unique linear Si oxide chains in high oxygen coverage regions. They also provide a natural explanation of the experimental observations that the S_B step with rebonds and DBs at its edge acts as a strong sink for the oxidation of Si.

ACKNOWLEDGMENTS

We gratefully acknowledge the support from the Korea

Research Foundation under Agreement No. KRF-2006-312-C00122 (B.D.Y.), the MOCIE of Korea through the National R&D Project for Nano Science and Technology (H.K., K.K., and I.-W.L.), the MOST of Korea through the Center for Atomic Wires and Layers (H.W.Y.), the Next Generation Supercomputer Project, MEXT Japan, Ministry of Science and Education (Y.M.), and the Seoul Science Fellowship (J.-N.Y.). The computations were performed at the UoSPCC-II facility at the Seoul Parallel Computation Center of the University of Seoul.

*Corresponding author. ybd@uos.ac.kr

[1] *Fundamental Aspects of Silicon Oxidation*, edited by Y. J. Chabal (Springer-Verlag, Berlin, 2001).
[2] T. Engel, Surf. Sci. Rep. **18**, 91 (1993).
[3] I.-W. Lyo and P. Avouris, Science **253**, 173 (1991).
[4] R. Martel, P. Avouris, and I.-W. Lyo, Science **272**, 385 (1996).
[5] T. Miyake, S. Soeki, H. Kato, T. Nakamura, A. Namiki, H. Kamba, and T. Suzaki, Phys. Rev. B **42**, 11801 (1990).
[6] R. Kliese, B. Rötter, D. Badt, and H. Neddermeyer (unpublished).
[7] H. W. Yeom, H. Hamamatsu, T. Ohta, and R. I. G. Uhrberg, Phys. Rev. B **59**, R10413 (1999).
[8] B. Ferguson, C. Reeves, and C. Mullins, J. Chem. Phys. **110**, 11574 (1999).
[9] T. Hoshino, M. Tsuda, S. Oikawa, and I. Ohdomari, Phys. Rev. B **50**, 14999 (1994).
[10] K. Hata, T. Kimura, S. Ozawa, and H. Shigekawa, J. Vac. Sci. Technol. A **18**, 1933 (2000).
[11] F. J. Grunthaner and P. J. Grunthaner, Mater. Sci. Rep. **1**, 65 (1986).
[12] J. A. Schaefer, F. Stucki, W. Goöpel, and G. L. Lapeyre, J. Vac. Sci. Technol. B **2**, 359 (1984).
[13] J. A. Schaefer and W. Göpel, Surf. Sci. **155**, 535 (1985).
[14] H. Ikeda, K. Hotta, T. Yamada, S. Zaima, and Y. Yasuda, Jpn. J. Appl. Phys., Part 1 **34**, 2191 (1995).
[15] P. Avouris and D. Cahill, Ultramicroscopy **42-44**, 838 (1992).
[16] D. G. Cahill and Ph. Avouris, Appl. Phys. Lett. **60**, 326 (1992).
[17] H. Ikegami, K. Ohmori, H. Ikeda, H. Iwano, Sh. Zaima, and Y. Yasuda, Jpn. J. Appl. Phys., Part 1 **35**, 1593 (1996).
[18] L. Incoccia, A. Balrna, S. Cramm, C. Kunz, F. Senf, and I. Storjohann, Surf. Sci. **189/190**, 453 (1994).
[19] H. Ibach, H. D. Bruchmann, and H. Wagner, Appl. Phys. A: Solids Surf. **29**, 113 (1982).
[20] J. R. Engstrom, D. J. Bonser, and T. Engel, Surf. Sci. **268**, 238 (1992).
[21] H. Watanabe, K. Kato, T. Uda, K. Fujita, M. Ichikawa, T. Kawamura, and K. Terakura, Phys. Rev. Lett. **80**, 345 (1998).
[22] T. Uchiyama and M. Tsukada, Phys. Rev. B **53**, 7917 (1996).
[23] T. Uchiyama and M. Tsukada, Phys. Rev. B **55**, 9356 (1997).
[24] T. Uchiyama, T. Uda, and K. Terakura, Surf. Sci. **433-435**, 896 (1999).
[25] K. Kato, T. Uda, and K. Terakura, Phys. Rev. Lett. **80**, 2000 (1998).
[26] K. Kato and T. Uda, Phys. Rev. B **62**, 15978 (2000).
[27] H. Kageshima and K. Shiraishi, Surf. Sci. **438**, 102 (1999).
[28] T. Yamasaki, K. Kato, and T. Uda, Phys. Rev. Lett. **91**, 146102 (2003).
[29] H. Kageshima and K. Shiraishi, Phys. Rev. Lett. **81**, 5936 (1998).
[30] B. D. Yu, Young Jin Kim, J. Jeon, H. Kim, H. W. Yeom, I.-W. Lyo, K. J. Kong, Y. Miyamoto, O. Sugino, and T. Ohno, Phys. Rev. B **70**, 033307 (2004).
[31] B. D. Yu, K. Park, H. Kim, C.-H. Chung, H. W. Yeom, I.-W. Lyo, K. Kong, Y. Miyamoto, O. Sugino, and T. Ohno, Jpn. J. Appl. Phys., Part 1 **45**, 2144 (2006).
[32] C.-H. Chung, H.-W. Yeom, B. D. Yu, and I.-W. Lyo, Phys. Rev. Lett. **97**, 036103 (2006).
[33] D. J. Chadi, Phys. Rev. Lett. **59**, 1691 (1987).
[34] T. Komura, M. Yoshimura, and T. Yao, J. Vac. Sci. Technol. B **14**, 906 (1996).
[35] T. Komura, T. Yao, and M. Yoshimura, Phys. Rev. B **56**, 3579 (1997).
[36] B. S. Swartzentruber, Phys. Rev. B **55**, 1322 (1997).
[37] P. Hohenberg and W. Kohn, Phys. Rev. **136**, B864 (1964); W. Kohn and L. J. Sham, Phys. Rev. **140**, A1133 (1965).
[38] D. Vanderbilt, Phys. Rev. B **41**, 7892 (1990).
[39] G. Kresse and J. Hafner, J. Phys.: Condens. Matter **6**, 8245 (1994).
[40] G. Kresse and J. Hafner, Phys. Rev. B **47**, R558 (1993).
[41] G. Kresse and J. Furthmuller, Phys. Rev. B **54**, 11169 (1996).
[42] J. P. Perdew, J. A. Chevary, S. H. Vosko, K. A. Jackson, M. R. Pederson, D. J. Singh, and C. Fiolhais, Phys. Rev. B **46**, 6671 (1992).
[43] A. Oshiyama, Phys. Rev. Lett. **74**, 130 (1995).
[44] S. Jeong and A. Oshiyama, Phys. Rev. Lett. **79**, 4425 (1997).
[45] T. Watanabe and I. Ohdomari, Appl. Surf. Sci. **162-163**, 116 (2000).
[46] K. Shiraishi, H. Kageshima, and M. Uematsu, Jpn. J. Appl. Phys., Part 2 **39**, L1263 (2000).
[47] S.-H. Lee and M.-H. Kang, Phys. Rev. Lett. **82**, 968 (1999).